# Delayed biological recovery from extinctions throughout the fossil record

**Article** *in* Nature · April 2000

DOI: 10.1038/35004564 · Source: PubMed



**2 authors**, including:

James W. Kirchner
ETH Zurich
**365** PUBLICATIONS **21,041** CITATIONS

SEE PROFILE

sensitive lakes. *J. Geophys. Res.* **100,** 25179–25204 (1995).
12. Birkett, C. M. Contribution of the TOPEX NASA radar altimeter to the global monitoring of large rivers and wetlands. *Wat. Resour. Res.* **34,** 1223–1239 (1998).
13. Mertes, L. A. K. Documentation and significance of the perirheic zone on inundated floodplains. *Wat. Resour. Res.* **33,** 1749–1762 (1997).
14. Smith, L. C. Satellite remote sensing of river inundation area, stage, and discharge: A review. *Hydrol. Processes* **11,** 1427–1439 (1997).
15. Mertes, L. A. K. *et al.* Spatial patterns of hydrology, geomorphology, and vegetation on the floodplain of the Amazon River in Brazil from a remote sensing perspective. *Geomorphology* **13,** 215–232 (1995).
16. Sippel, S. J., Hamilton, S. K., Melack, J. M. & Novo, E. M. M. Passive microwave observations of inundation area and the area/stage relation in the Amazon River floodplain. *Int. J. Remote Sensing* **19,** 3055–3074 (1998).
17. Peltzer, G. & Rosen, P. Surface displacement of the 17 May 1993 Eureka Valley, California, earthquake observed by SAR interferometry. *Science* **268,** 1333–1336 (1995).
18. Wicks, C., Thatcher, W. & Dzurisin, D. Migration of fluids beneath Yellowstone caldera inferred from satellite radar interferometry. *Science* **282,** 458–462 (1998).
19. Burgmann, R., Fielding, E. & Sukhatme, J. Slip along the Hayward fault, California, estimated from space-based synthetic aperture radar interferometry. *Geology* **26,** 559–562 (1998).
20. Rignot, E. J., Gogineni, S. P., Krabill, W. B. & Ekholm, S. North and northeast Greenland ice discharge from satellite radar inteferometry. *Science* **272,** 934–937 (1997).
21. Joughin, I., Kwok, R. & Fahnestock, M. Estimation of ice-sheet motion using satellite radar interferometry: Method and error analysis with application to Humboldt Glacier, Greenland. *J. Glaciol.* **42,** 564–575 (1996).
22. Li, F. K. & Goldstein, R. M. Studies of multibaseline spaceborne interferometric synthetic aperture radars. *IEEE Trans. Geosci. Remote Sensing* **28,** 88–97 (1990).
23. Zebker, H. A. & Villasenor, J. Decorrelation in interferometric radar echoes. *IEEE Trans. Geosci. Remote Sensing* **30,** 950–959 (1992).
24. Rosen, P. A., Hensley, S., Zebker, H. A., Webb, F. H. & Fielding, E. J. Surface deformation and coherence measurements of Kilauea Volcano, Hawaii, from SIR-C radar interferometry. *J. Geophys. Res.* **101,** 23109–23125 (1996).
25. Massonnet, D. & Rabaute, T. Radar interferometry: Limits and potential. *IEEE Trans. Geosci. Remote Sensing* **31,** 455–464 (1993).
26. Zebker, H. A., Rosen, P. A., Hensley, S. & Mouginis-Mark, P. J. Analysis of active lava flows on Kilauea volcano, Hawaii, using SIR-C radar correlation measurements. *Geology* **24,** 495–498 (1996).
27. Rignot, E. Dual-frequency interferometric SAR observations of a tropical rain-forest. *Geophys. Res. Lett.* **23,** 993–996 (1996).

**Acknowledgements**

We thank H. Zebker, C. Birkett and J. Ridley for comments on the manuscript. The Cornell Theory Center provided the computer resources necessary for SAR processing. Gamma Remote Sensing Research and Consulting provided SAR technical advice. This work was supported by NASA.

Correspondence and requests for materials should be addressed to D.E.A. (e-mail: alsdorf@icess.ucsb.edu).

# Delayed biological recovery from extinctions throughout the fossil record

**James W. Kirchner* & Anne Weil†**

* *Department of Geology and Geophysics, University of California, Berkeley, California, 94720-4767, USA*
† *Department of Biological Anthropology and Anatomy, Duke University, Durham, North Carolina 27708-0383, USA*

**How quickly does biodiversity rebound after extinctions? Palaeobiologists have examined the temporal, taxonomic and geographic patterns of recovery following individual mass extinctions in detail[1–5], but have not analysed recoveries from extinctions throughout the fossil record as a whole. Here, we measure how fast biodiversity rebounds after extinctions in general, rather than after individual mass extinctions, by calculating the cross-correlation between extinction and origination rates across the entire Phanerozoic marine fossil record. Our results show that extinction rates are not significantly correlated with contemporaneous origination rates, but instead are correlated with origination rates roughly 10 million years later. This lagged correlation persists when we remove the 'Big Five' major mass extinctions, indicating that recovery times following mass extinctions and background extinctions are similar. Our results suggest that there are intrinsic limits to how quickly global biodiversity can recover after extinction events, regardless of their magnitude. They also imply that today's anthropogenic extinctions will diminish biodiversity for millions of years to come.**

A key component of biotic recovery is the time lag between episodes of rapid extinction and subsequent periods of rapid origination. Originations rebuild biodiversity, and origination rates are commonly assumed to peak when ecosystems have recovered sufficient diversity to inhibit further diversification[6]. Thus, the elapsed time between extinction rate peaks and origination rate peaks is one measure of the recovery time (Fig. 1). We can estimate the average time lag for the whole fossil record using the cross-correlation between extinctions and originations, which measures how closely the two time series resemble each other, when one is shifted forwards or backwards by a specified interval. For regularly spaced time series, the cross-correlation function could be calculated as

$$r_{EO}(k) = \frac{\Sigma(E_i - \bar{E}_i)(O_j - \bar{O}_j)}{\sqrt{\Sigma(E_i - \bar{E}_i)^2}\sqrt{\Sigma(O_j - \bar{O}_j)^2}}, \quad j = i + k \qquad (1)$$

where $E$ and $O$ are the extinction and origination time series, and $r_{EO}(k)$ is their cross-correlation when originations lag extinctions by $k$ steps. This direct approach cannot be applied to the fossil record, because its stratigraphic boundaries are unevenly spaced in time. Nor should one simply even out the spacing by interpolating within each stratigraphic interval, because this introduces artefactual correlation among the interpolated points[7,8]. Instead, we use equation (1) to calculate the correlation between all pairs of points $E_i$ and $O_j$ whose separations in time, $t_j - t_i$, fall within 5 Myr bins of lag time (rather than points separated by fixed numbers of steps); this yields a geostatistical approximation to the cross-correlation function[9] (Fig. 2a, b). A second approach to calculating the cross-correlation between two unevenly spaced time series is through their Fourier transforms[10,11]:

$$r_{EO}(\tau) = FT^{-1}(FT\{E\}FT^{*}\{O\}) \qquad (2)$$

where $FT$, $FT^*$ and $FT^{-1}$ denote the Fourier transform, its complex conjugate and its inverse, respectively, and $r_{EO}(\tau)$ is the cross-correlation between $E$ and $O$ at a lag of $\tau$ Myr (Fig. 2c, d). We use the Lomb–Scargle Fourier transform[11–14] to calculate $FT\{E\}$ and $FT^*\{O\}$ directly from the unevenly spaced fossil data, without interpolation. The Lomb–Scargle algorithm has similar statistical properties, when applied to unevenly spaced data, to those of conventional Fourier transform algorithms when applied to evenly spaced data[14].

Our source data are Sepkoski's compilations of fossil marine animal genera[15] and families[16], with revisions through 1997. Because long-term drift could obscure the cross-correlations that we seek to analyse, we subtracted the long-term trends (shown as dotted lines in Fig. 1b, c) from the extinction and origination time series before analysis.

The resulting cross-correlation functions (Fig. 2) show that extinctions and originations are not significantly correlated over short lag periods, indicating that, on average, extinctions do not trigger immediate evolutionary rebounds. Instead, the cross-correlation is strongest when originations lag extinctions by roughly 10 Myr. This indicates that the average interval between extinction peaks and origination peaks, and thus the average recovery time from extinctions, is about 10 Myr across the fossil record. The statistical significance of these cross-correlations—that is, the chance of correlations this strong arising by chance at any lag, from −15 to 35 Myr—is $P < 0.05$ for all but one of the 16 cases shown in Fig. 2 (see Supplementary Information). The peak cross-correlation occurs at similar lags with either calculation method, and in both the genus and family data sets, indicating that this result

is robust.

To test whether these results are driven by the mass extinctions, we repeated our analysis after excluding the 'Big Five' extinction peaks (Fig. 1) from the data set. The resulting cross-correlations (heavy dotted lines, Fig. 2) are weaker, but still have their strongest positive values when originations lag extinctions by roughly 10 Myr. We also rank-transformed the extinction and origination rates to obtain a cross-correlation function, analogous to the Spearman rank correlation, that minimizes the influence of extreme values associated with mass extinctions. The results of this analysis (dashed

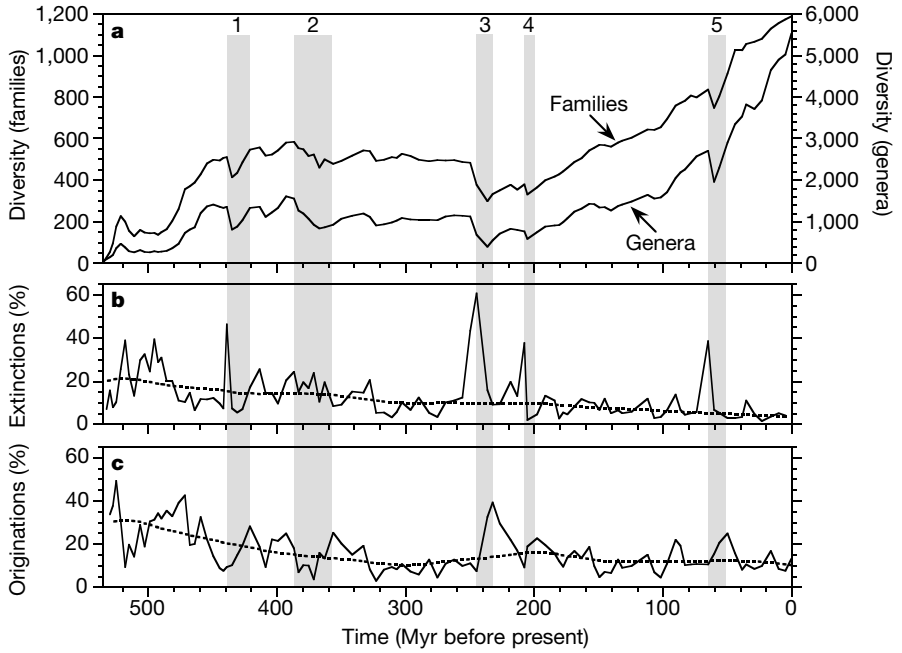


**Figure 1** The fossil record of marine animal biodiversity. Standing diversity of genera and families through the Phanerozoic (**a**), and corresponding percentages of extinction (**b**) and origination (**c**) of genera in each stratigraphic interval. Shaded bands highlight recovery intervals (between extinction rate peaks and subsequent origination rate peaks) for the 'Big Five' mass extinctions: end-Ordovician (1), late Devonian (2), end-Permian (3), end-Triassic (4) and Cretaceous–Tertiary (5). Dotted lines in **b** and **c** show the long-term trends (estimated using LOWESS, a robust curve-fitting technique[19]) that are subtracted from extinction and origination time series before calculating cross-correlations.

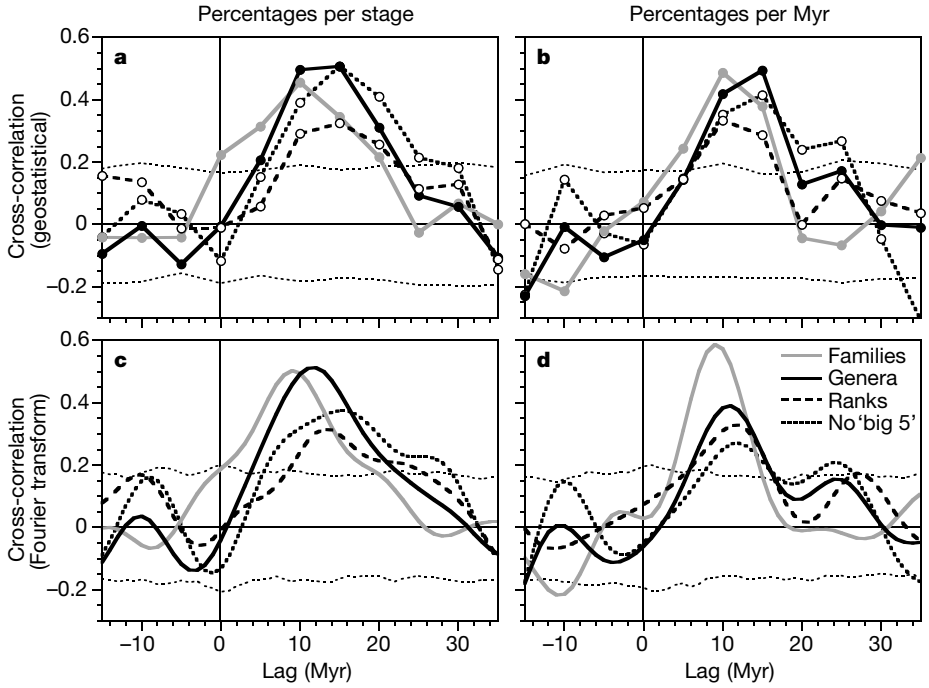


**Figure 2** Cross-correlation between extinctions and originations. Cross-correlation functions calculated by geostatistical (**a**, **b**) and Fourier transform (**c**, **d**) methods, from percentage rates of extinction and origination per stratigraphic interval (**a**, **c**) and per million years (**b**, **d**). Cross-correlations are shown for genera (black lines), families (grey lines), rank-transformed genera (dashed lines) and genera with the 'Big Five' major mass extinctions removed (heavy dotted lines). Fine dotted lines indicate upper and lower 5% confidence bounds for uncorrelated time series, calculated from cross-correlations of 1,000 random shuffles of the original data. Positive lags indicate originations lagging extinctions.

lines, Fig. 2) are similar to those obtained by deleting the 'Big Five' events. Considered together, these results indicate that recovery times on the order of 10 Myr, previously noted for mass extinctions[3–5], are also characteristic of background extinctions.

The incompleteness of the fossil record implies that last occurrences of fossils, and thus apparent extinctions, are earlier than actual dates of extinction[17] (the Signor–Lipps effect); it also implies that first occurrences of fossils, and thus apparent originations, are later than actual dates of origination[5] (the 'Sppil–Rongis' effect). Could these two artefacts create lagged correlations similar to those that we observe? We tested this possibility by assuming that originations at each stage boundary were exactly equal to extinctions—thus creating perfectly correlated records, with no lag—and then spreading apparent extinctions backwards in time and apparent originations forwards in time, as one would expect from incomplete sampling (see Methods). Figure 3 shows that even a very incomplete fossil record, with average intervals of 5 or 10 Myr between fossil discoveries, would not produce lagged correlations similar to those we observed: smearing the fossil record stretches the cross-correlation function toward longer lags, but does not shift its peak. Therefore, the lagged cross-correlation in the real fossil data cannot be explained by incomplete sampling of the fossil record.

As similar recovery intervals appear to follow both mass extinctions and background extinctions, the timescale of recovery may be determined not by the magnitude of individual extinctions, but instead by the internal dynamics of the diversification process. Species do not merely occupy ecological niches; they also serve as evolutionary starting points for radiation into additional niches, and they themselves constitute niches for their predators, parasites and symbionts. Consequently, as extinctions eliminate species they also destroy niches, and may thus reduce biodiversity without creating many evolutionary opportunities. Instead, new opportunities for radiation may arise mostly from diversification itself, which, in creating new taxa, creates new niches and new evolutionary pathways into existing niches. This implies that, after extinctions, origination rates should initially be low, accelerating only as diversification creates niche space, and finally peaking when ecosystem structure is sufficiently developed to slow further diversification. The duration of this process, and thus the recovery timescale, will depend on the structure of the post-extinction ecosystem, which will be configured differently than the pre-extinction ecosystem. If the structure of the new ecosystem depends on biogeographic and taxonomic factors[2], the duration of the recovery process may be largely independent of extinction magnitude. Thus, although mass extinctions are larger than background extinctions, we should not expect their recoveries to be proportionally or consistently longer.

Multimillion-year recovery intervals are a previously unrecognized general property of the fossil record, not a phenomenon associated only with mass extinctions. Our results suggest that there are intrinsic 'speed limits' that regulate recovery from small extinctions as well as large ones. Thus, today's anthropogenic extinctions are likely to have long-lasting effects, whether or not they are comparable in scope to the major mass extinctions. Even if *Homo sapiens* survives several million more years, it is unlikely that any of our species will see biodiversity recover from today's extinctions. □

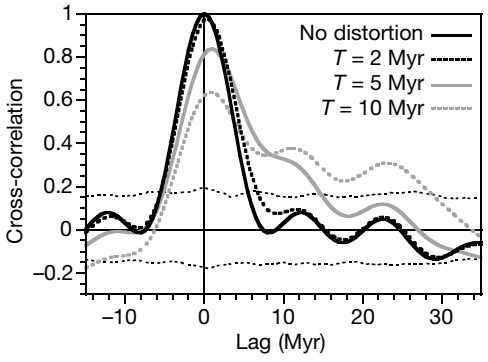


**Figure 3** Effect of incomplete sampling. Cross-correlation functions (calculated by Fourier transform method) are shown for synthetic, perfectly correlated extinction and origination time series, with and without distortion by simulated Signor–Lipps and 'Sppil–Rongis' effects (see Methods). Curves are shown for different degrees of distortion, corresponding to different average intervals *T* between fossil discoveries in each taxon. Backwards-smearing of extinctions and forwards-smearing of originations do not shift the peak cross-correlation, but instead stretch the cross-correlation function toward longer lags.

## Methods

### Source data

Sepkoski's timescale aggregates some stratigraphic stages and subdivides others, yielding 106 intervals, 2.5 to 12.5 Myr in length, from the Cambrian through the Pleistocene. To minimize Lagerstätten and monographic effects[15], we excluded all taxa that occur in only one stratigraphic interval. We analysed originations and extinctions as percentages per stratigraphic interval (originations or extinctions divided by total diversity in each interval) and percentages per unit time (originations or extinctions divided by total diversity and interval length)[18]. Our family cross-correlations (grey lines, Fig. 2) exclude the Cambrian, because its low initial familial diversity yields anomalously high percentages of extinctions and originations. We assigned originations in each interval to the stratigraphic boundary that begins it, and extinctions to the stratigraphic boundary that ends it; this approach is conservative because it minimizes the time by which originations lag extinctions. To the extent that faunal turnover occurred within (rather than between) stratigraphic intervals, and thus extinctions and originations within each interval were highly correlated, our procedure would yield an artefactual negative lag (that is, extinctions lagging originations), the opposite of what we observe. Assigning originations and extinctions to the midpoint of each stratigraphic interval would lengthen the lag between extinctions and subsequent originations by roughly the average interval length (5 Myr), but would not significantly change the shape of the cross-correlation functions (see Supplementary Information).

### Simulating incomplete sampling

If fossil discoveries from a given genus or family are randomly distributed through time (a Poisson process), the interval $\Delta t$ between the actual time of origination and the first fossil found (or between the actual time of extinction and the last fossil found) will follow an exponential probability distribution:

$$p(\Delta t) = \frac{1}{T} e^{-\Delta t/T} \quad (3)$$

where $T$ is the average interval between individual fossil discoveries from each genus or family. The apparent extinction or origination time series can be estimated by convolving equation (3) with the actual time series of extinctions or originations.

Received 30 September 1999; accepted 5 January 2000.


1. Hallam, A. Why was there a delayed radiation after the end-Palaeozoic extinctions? *Hist. Biol.* **5,** 257–262 (1991).
2. Jablonski, D. Geographic variation in the molluscan recovery from the end-Cretaceous extinction. *Science* **279,** 1327–1330 (1998).
3. Jablonski, D. in *Extinction Rates* (eds Lawton, J. H. & May, R. M.) 25–44 (Oxford Univ. Press, New York, 1995).
4. Erwin, D. H. The end and the beginning: recoveries from mass extinctions. *Trends Ecol. Evol.* **13,** 344–349 (1998).
5. Sepkoski, J. J. Jr Rates of speciation in the fossil record. *Phil. Trans. R. Soc. Lond. B* **353,** 315–326 (1998).
6. Walliser, O. H. in *Global Events and Event Stratigraphy in the Phanerozoic* (ed. Walliser, O. H.) 7–19 (Springer, Berlin, 1996).
7. Kirchner, J. W. & Weil, A. No fractals in fossil extinction statistics. *Nature* **395,** 337–338 (1998).
8. Schulz, M. & Stattegger, K. SPECTRUM: Spectral analysis of unevenly spaced paleoclimatic time series. *Comput. Geosci.* **23,** 929–945 (1997).
9. Agterberg, F. P. in *Geostatistics* (ed. Merriam, D. F.) 113–141 (Plenum, New York, 1970).
10. Bracewell, R. N. *The Fourier Transform and its Applications* 3rd edn (McGraw Hill, Boston, 2000).
11. Scargle, J. D. Studies in astronomical time series analysis. III. Fourier transforms, autocorrelation functions, and cross-correlation functions of unevenly spaced data. *Astrophys. J.* **343,** 874–887 (1989).
12. Lomb, N. R. Least-squares frequency analysis of unequally spaced data. *Astrophys. Space Sci.* **29,** 447–462 (1976).
13. Press, W. H. & Teukolsky, S. A. Search algorithm for weak periodic signals in unevenly spaced data. *Comput. Phys.* **2,** 77–82 (1988).
14. Scargle, J. D. Studies in astronomical time series analysis. II. Statistical aspects of spectral analysis of unevenly spaced data. *Astrophys. J.* **263,** 835–853 (1982).
15. Sepkoski, J. J.Jr in *Global Events and Event Stratigraphy in the Phanerozoic* (ed. Walliser, O. H.) 35–51 (Springer, Berlin, 1996).
16. Sepkoski, J. J.Jr Ten years in the library: new data confirm paleontological patterns. *Paleobiology* **19,** 43–51 (1993).
17. Signor, P. W. & Lipps, J. H. Sampling bias, gradual extinction patterns, and catastrophes in the fossil record. *Geol. Soc. Am. Special Paper* **190,** 291–296 (1982).

18. Gilinsky, N. L. in *Analytical Paleobiology* (eds Gilinsky, N. L. & Signor, P. W.) 157–174 (The Paleontological Society, Knoxville, Tennessee, 1991).
19. Cleveland, W. S. & McGill, R. The many faces of a scatterplot. *J. Am. Stat. Assoc.* **79,** 807–822 (1984).

**Supplementary information** is available on *Nature*'s World-Wide Web site (http://www.nature.com) or as paper copy from the London editorial office of *Nature*.

**Acknowledgements**

We are indebted to the late J. Sepkoski for his fossil databases and his encouragement, and we thank M. Foote and D. Erwin for comments on the manuscript. Our work was supported by grants from the University of California and the NSF to J.W.K.

Correspondence and requests for materials should be addressed to J.W.K. (e-mail: kirchner@seismo.berkeley.edu)

# Simple rules yield complex food webs

**Richard J. Williams & Neo D. Martinez**

*Romberg Tiburon Center, Department of Biology, San Francisco State University, PO Box 855, Tiburon, California 94920, USA*

**Several of the most ambitious theories in ecology[1–14] describe food webs that document the structure of strong and weak trophic links[9] that is responsible for ecological dynamics among diverse assemblages of species[4,11–13]. Early mechanism-based theory asserted that food webs have little omnivory and several properties that are independent of species richness[1–4,6]. This theory was overturned by empirical studies that found food webs to be much more complex[5,7–9,14–18], but these studies did not provide mechanistic explanations for the complexity[9]. Here we show that a remarkably simple model fills this scientific void by successfully predicting key structural properties of the most complex and comprehensive food webs in the primary literature. These properties include the fractions of species at top, intermediate and basal trophic levels, the means and variabilities of generality, vulnerability and food-chain length, and the degrees of cannibalism, omnivory, looping and trophic similarity. Using only two empirical parameters, species number and connectance, our 'niche model' extends the existing 'cascade model'[3,19] and improves its fit ten-fold by constraining species to consume a contiguous sequence of prey in a one-dimensional trophic niche[20].**

We compare the abilities of two earlier models, the random and cascade models[3,19], and our new niche model to predict a dozen properties for each of seven food webs. The parameters of all models are set to synthesize webs with the empirically observed species number and connectance level. We compare model predictions with the largest and highest-quality empirical food webs that include autotrophs and were originally documented to study food web structure comprehensively (Table 1). Three are from freshwater habitats: Skipwith Pond, Little Rock Lake and Bridge Brook Lake; two are from habitats at freshwater-marine interfaces: Chesapeake Bay and Ythan Estuary; and two are from terrestrial habitats: Coachella Valley and the island of St Martin.

**Table 1 Basic properties of empirical food webs**

| Name | Taxa | $S$ | $L/S$ | $C(L/S^2)$ |
|---|---|---|---|---|
| Skipwith Pond | 35 | 25 | 7.9 | 0.32 |
| Little Rock Lake | 181 | 92 | 10.8 | 0.12 |
| Bridge Brook Lake | 75 | 25 | 4.3 | 0.17 |
| Chesapeake Bay | 33 | 31 | 2.2 | 0.072 |
| Ythan Estuary | 92 | 78 | 4.8 | 0.061 |
| Coachella Valley | 30 | 29 | 9.0 | 0.31 |
| St Martin Island | 44 | 42 | 4.9 | 0.12 |

'Taxa' refers to the original names for groups of organisms found in the primary reference. ***S*** refers to trophic species[3]. The seven food webs address (1) primarily invertebrates in Skipwith Pond[15]; (2) pelagic and benthic species in Little Rock Lake[17], the largest food web in the primary literature; (3) Bridge Brook Lake, the largest among a recent set of 50 Adirondak lake pelagic food webs[6,7]; (4) the pelagic portion of Chesapeake Bay emphasizing larger fishes[30]; (5) mostly birds and fishes among invertebrates and primary producers in the Ythan Estuary[16]; (6) a wide range of highly aggregated taxa in the Coachella desert[5]; and (7) trophic interactions emphasizing *Anolis* lizards on the Caribbean island of St Martin[18].

Throughout this work, 'species' refers to trophic species, which are functional groups of taxa that share the same predators and prey in a food web[3]. 'Trophic species' is a widely accepted[3,4,8,14,17,18] and sometimes criticized convention[5,14] within structural food-web studies that reduces methodological biases in the data[3,4,8]. A matrix with $S$ rows and columns represents a food web with $S$ species. Element $a_{ij}$ is 1 if species $j$ consumes species $i$ and 0 if not. There are $S^2$ possible and $L$ actual links. Directed connectance[17] ($C$) equals $L/S^2$.

In the random model[3,19], any link among $S$ species occurs with the same probability ($P$) equal to $C$ of the empirical web. This creates webs as free as possible from biological structuring while maintaining the observed $S$ and $C$. The cascade model[3,19] assigns each species a random value drawn uniformly from the interval [0,1] and each species has probability $P = 2CS/(S-1)$ of consuming only species with values less than its own. This pecking order helps to explain species richness among trophic levels[3] but underestimates interspecific trophic similarity[19] and overestimates food-chain length and number in larger webs[3,18]. The niche model (Fig. 1) similarly assigns each species a randomly drawn 'niche value'. The species are then constrained to consume all prey species within one range of values whose randomly chosen centre is less than the consumer's niche value. The single range adds a previously discussed[20] community-level contiguity of niche space to the cascade model by causing species with similar niche values to share consumers frequently within the community. The placement of the niche partially relaxes the cascade hierarchy by allowing up to half a consumer's range to include species with niche values higher than the consumer's value. All three models incorporate substantial stochastic variability along with dependence on $S$ and $C$.

Twelve properties of each empirical and model web are measured (see Methods):
(i–iii) Species types[1–8,14–18,21]: the fractions of top (***T***, species with no predators), intermediate (***I***, species with both predators and prey) and basal (***B***, species with no prey) species.
(iv, v) The standard deviations (s.d.) of generality[14] (*GenSD*) and vulnerability[14] (*VulSD*) quantify the respective variabilities of species' normalized prey ($G_i$) and predator ($V_i$) counts:

$$G_i = \frac{1}{L/S}\sum_{j=1}^{S} a_{ji} \qquad V_i = \frac{1}{L/S}\sum_{j=1}^{S} a_{ij}$$

Normalizing with $L/S$ makes s.d. comparable across different webs by forcing mean $G_i$ and $V_i$ to equal 1.

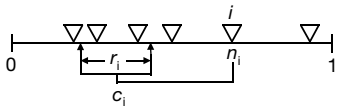


**Figure 1** Diagram of the niche model. Each of $S$ species (for example, $S = 6$, each shown as an inverted triangle) is assigned a 'niche value' parameter ($n_i$) drawn uniformly from the interval [0,1]. Species ***i*** consumes all species falling in a range ($r_i$) that is placed by uniformly drawing the centre of the range ($c_i$) from [$r_i$/2, $n_i$]. This permits looping and cannibalism by allowing up to half of $r_i$ to include values $\geq n_i$. The size of $r_i$ is assigned by using a beta function to randomly draw values from [0,1] whose expected value is $2C$ and then multiplying that value by $n_i$ [expected E($\eta$) = 0.5] to obtain the desired $C$. A beta distribution with $\alpha = 1$ has the form $f(x|1, \beta) = \beta(1-x)^{\beta-1}$, $0 < x < 1$, 0 otherwise, and $E(X) = 1/(1+\beta)$. In this case, $x = 1-(1-y)^{1/\beta}$ is a random variable from the beta distribution if $y$ is a uniform random variable and $\beta$ is chosen to obtain the desired expected value. We chose this form because of its simplicity and ease of calculation. The fundamental generality of species $i$ is measured by $r_i$. The number of species falling within $r_i$ measures realized generality. Occasionally, model-generated webs contain completely disconnected species or trophically identical species. Such species are eliminated and replaced until the web is free of such species. The species with the smallest $n_i$ has $r_i = 0$ so that every web has at least one basal species.